Thin–Walled Structures 146 (2020) 106472

Contents lists available at ScienceDirect

Thin-Walled Structures

journal homepage: http://www.elsevier.com/locate/tws

Full length article

Strength and stability of spherical-conical shell assemblies under external hydrostatic pressure

Alphose Zingoni *, Nosakhare Enoma

Department of Civil Engineering, University of Cape Town, Rondebosch, 7701, Cape Town, South Africa

ARTICLE INFO

Keywords:
Shell structure
Shell of revolution
Spherical-conical shell
Hydrostatic pressure
Shell analysis
Shell buckling

ABSTRACT

Thin shells are increasingly finding new applications under the sea. In this study, we consider a thin-walled shell-of-revolution assembly comprising a deep spherical shell dome (deeper than a hemisphere) axisymmetrically and tangentially joined to a steep-sided conical shell, the whole being a closed shell structure intended for stationary deployment beneath the surface of the sea in relatively shallow water. The closed shell structure, which might serve as an underwater observatory, is intended to operate at a constant depth, anchored to the seabed against flotation forces, with the thin steel shell walls being required to withstand the external hydrostatic pressure of the surrounding water. We use shell theory to investigate the discontinuity stresses that occur at the junction of the spherical shell and the conical shell, and employ FEM to explore the buckling behaviour of the thin shell. While discontinuity stresses are relatively small, they may influence the lower buckling modes of the shell, which are found to be largely confined to the region of the cone that is adjacent to the junction. Considerations are extended to a doubly-curved variant of the cone in the form of a paraboloid of revolution. As expected, double curvature enhances buckling capacity and also influences the mode shapes.

1. Introduction

Industrial applications of thin shells of revolution range from boilers and pressure vessels to storage vessels for water, chemicals, oil and liquefied gases [1]. Strength and stability are major considerations in designing liquid-containment shells of revolution [2] as well as pressure vessels. Under service conditions, linear shell theory provides a good estimate of the state of stress in the shell, with the membrane theory being particularly useful for regions of the shell that are free of discontinuities in geometry or loading, and the bending theory being of more general applicability [3,4]. For regions of the shell that are close to lines of support, concentrated loadings, discontinuities in surface loading, discontinuities in shell geometry and shell junctions, the membrane theory (which assumes bending effects in the shell are negligible) is not valid, and resort must be made to the bending theory.

In general, where there is a co-existence of membrane and bending effects, a convenient approach in the linear elastic analysis of axisymmetrically loaded shells of revolution is to regard the membrane solution as the particular integral of the governing differential equations, and adopt a set of axisymmetric edge forces and bending moments as the homogeneous solution accounting for the so-called "edge effect". This approach has been successfully used in analytical studies of various shell-discontinuity problems [5–9]. Other studies specific to shell junctions may be seen in a recent review [10]. In thin shells of revolution of zero or positive Gaussian curvature, if the shell is not too shallow, it is found that discontinuity effects have an oscillatory and decaying character, quickly dying out with distance from the discontinuity. This behaviour permits the use of simplified bending theory [4].

When the principal loading on the shell is externally applied uniform or hydrostatic pressure, considerable compressive actions arise within the shell, and if the shell is very thin as is usually the case for metal shells, these actions may result in buckling of the shell. Buckling of shells of revolution under external pressure has been the subject of many studies. Von Karman and Tsien [11] studied the buckling of spherical shells, Singer [12] the buckling of circular conical shells, Seide [13] the buckling of truncated conical shells, and Sobel and Flügge [14] the stability of toroidal shells, all being under uniform external pressure. Similar studies for ellipsoidal shells may be seen in the review of Krivoshapko [15]. Various aspects of the buckling of thin shells were covered in the review of Teng [16]. In thin metal tanks of the type used for oil storage, buckling of the shell can be caused by the effects of external wind pressure or the existence of an internal vacuum [17–19],

* Corresponding author.
E-mail address: alphose.zingoni@uct.ac.za (A. Zingoni).

https://doi.org/10.1016/j.tws.2019.106472
Received 19 December 2018; Received in revised form 13 October 2019; Accepted 23 October 2019
Available online 9 November 2019

while in subsea shell applications [20–22], buckling is caused primarily by external hydrostatic pressure. The effects of external pressure on the stability of thin shells has also been extended to certain unusual geometries that offer enhanced structural characteristics [23,24].

In this paper, the original version of which was presented at the Eight International Conference on Thin-Walled Structures [25], we study thin-walled shell-of-revolution assemblies comprising a deep spherical shell dome (deeper than a hemisphere) axisymmetrically and tangentially joined to a steep-sided conical shell, the whole being a closed shell structure intended for stationary deployment beneath the surface of the sea in relatively shallow water. When deployed, the axis of revolution of the shell assembly is vertical, with the spherical dome being uppermost and the vertex of the conical shell being lowermost, this shape resembling that of a descending parachute or an ascending hot-air balloon. The closed shell structure is intended to operate at a constant depth, anchored to the seabed against flotation forces, with the thin steel shell walls being required to withstand the external hydrostatic pressure of the surrounding water.

First, we use linear elastic shell theory to investigate, in general terms, the discontinuity stresses that occur at the junction of the spherical shell and the conical shell. A formulation that takes into account membrane and bending effects is developed, and the results for stresses around the junction presented in closed-form. The accuracy of the formulation is verified by a finite-element analysis of the same problem based on numerical examples. Then for these numerical examples, we employ the Finite-Element Method (FEM) to perform a linear eigenvalue buckling analysis of the thin shell, which yields the buckling pressures and corresponding mode shapes. The same buckling analysis is carried out for a vessel where the conical shell has been replaced with its inscribed paraboloid of revolution, thus allowing the effect of double curvature on the bucking resistance of the lower shell to be evaluated.

Fig. 1(a) shows the geometrical parameters of the spherical-conical shell structure. For the spherical shell (comprising the upper part of the structure), the radius of the shell is denoted by a, while the meridional-angle coordinate (i.e. the angle between the axis of revolution of the assembly and the normal to the shell midsurface at the point in question) is denoted by ϕ; the value of ϕ at the edge of the spherical shell is denoted by ϕ_e. For the conical shell (comprising the lower part of the structure), the angle at the base of the cone is denoted by α (clearly $\alpha = \pi - \phi_e$ since the conical sides meet the spherical shell tangentially), while the distance coordinate (measured from the vertex of the cone along a sloping meridian) is denoted by s; the value of s at the edge of the cone is denoted by l (length of cone). The closed assembly is subjected to an external pressure of magnitude p.

Fig. 1(b) shows the same vessel with the conical shell now replaced with a paraboloid of revolution that has the same slope as the conical shell at the junction with the spherical shell. Discontinuity effects aside, the parabolic profile affords a shell geometry that is suited to containment and efficient in resisting applied surface loads through membrane action [26,27]. With the origin taken at the bottom of the vessel and the y coordinate measured upwards along the axis of revolution, the equation of the meridian of the paraboloid is given by

$$y = kx^2 \tag{1}$$

The constant k is given by the condition that the first derivative of equation (1) (i.e. $2kx$) at the value of x corresponding to the base of the cone (i.e. at $x = a\sin\alpha$) is equal to the slope of the cone (i.e. $k\tan\alpha$). The depth h of the paraboloid of revolution follows from equation (1) with k now known. The replacement of the conical shell with the paraboloid of revolution thus represents a loss in structural depth of $((l\sin\alpha) - h)$ or $((a\tan\alpha\sin\alpha) - h)$.

The present paper focuses on analytical stress evaluation and linear eigenvalue buckling analysis. The justification for a linear stress analysis is that a determination of the distribution and severity of elastic stresses under normal service conditions is an important first step in strength evaluations for new shell proposals, as this provides insight on whether or not buckling should be a concern (depending on the magnitude of the calculated compressive stresses), and if so, where the largest compressive stresses occur. This is in line with the classical approach [3]. Similarly, a linear buckling analysis provides a useful indication of the load level at which the shell becomes unstable, assuming linear-elastic material behaviour and small-deformation behaviour prior to the onset of buckling, and also ignoring the presence of imperfections for the

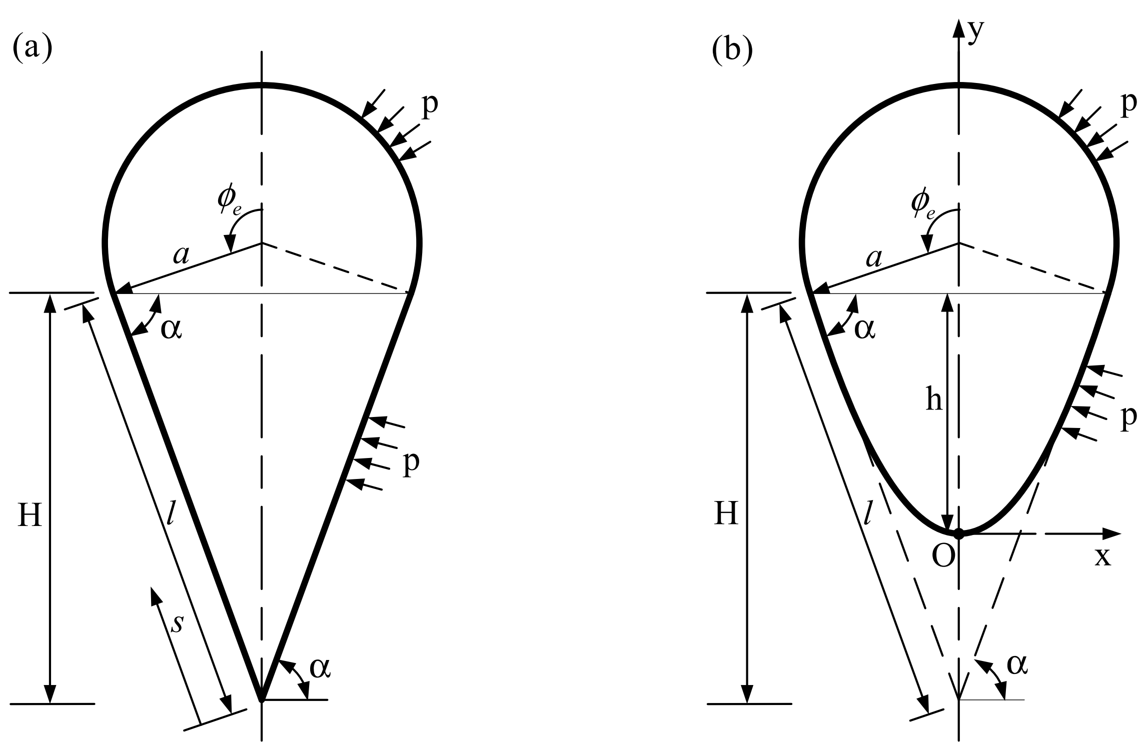

Fig. 1. Geometrical parameters of the shell structure: (a) spherical-conical assembly; (b) spherical-paraboloidal assembly.

time being (imperfections will form the subject of future work).

The buckling load calculated in this way is, of course, not necessarily the collapse load; in reality, the shell may either fail abruptly as soon as buckling has occurred, or it may continue to carry an increasing amount of load while sustaining more severe deformations (a behaviour that is highly nonlinear), until it eventually collapses. We are currently extending the study of the vessels in question to take into account non-linearity effects, postbuckling and collapse behaviour. The results of this ongoing work will be published in a follow-up article.

While geometric imperfections are known to have a strong influence on the buckling behaviour of thin containment shells, they are not taken into account in the first phase of this study. The aim is to first understand the behaviour of the perfect shell before we take into account geometric imperfections. The sensitivity of the buckling behaviour of the shell to the shape and size of likely imperfections will form the subject of future work. Finally, the scope of the present investigation does not extend to middle-thickness shells used in deep sea water.

2. Membrane stress resultants and deformations

Membrane theory yields the following general solutions for arbitrary shells of revolution [28]:

$$N_\phi = \frac{1}{r_2 \sin^2 \phi} \int r_1 r_2 (p_r \cos \phi - p_\phi \sin \phi) \sin \phi \; d\phi + k \tag{2a}$$

$$N_\theta = r_2 p_r - \frac{r_2}{r_1} N_\phi \tag{2b}$$

$$\delta = \frac{1}{Et}(r_2 \sin \phi)(N_\theta - \nu N_\phi) \tag{2c}$$

$$V = \frac{1}{r_1}\left[\frac{\cot \phi}{Et}\{(r_1 + \nu r_2)N_\phi - (r_2 + \nu r_1)N_\theta\} - \frac{d}{d\phi}\left\{\frac{r_2}{Et}(N_\theta - \nu N_\phi)\right\}\right] \tag{2d}$$

where N_ϕ and N_θ are the stress resultants (forces per unit length) in the meridional and hoop directions, respectively, of the shell of revolution. The parameter δ is the displacement of a point on the shell midsurface in the direction perpendicular to the axis of revolution of the shell (considered positive when away from the axis of revolution), while V is the rotation of the shell in the meridional section (considered positive when anticlockwise on the left-hand side of the axis of revolution). The positive directions of δ and V may be visualised by reference to Fig. 2, which shows the lateral displacements and rotations at the shell edges. The parameters p_r and p_ϕ are loading components (per unit area of the shell midsurface) in the direction normal to the shell midsurface (positive when outward) and the direction of the tangent to the meridian at a given point. The parameters r_1 and r_2 are the principal radii of curvature of the shell midsurface in the meridional plane, and in the plane perpendicular to the meridional plane and containing the normal at the point in question. Lastly, t denotes shell thickness, while E and ν denote Young's modulus and Poisson's ratio respectively.

For the special case of conical shells, owing to the vanishing of the meridional curvature, the second of the above equations degenerates into an explicit solution for N_θ in terms of p_r. With the angular coordinate ϕ of the general shell of revolution now replaced with the distance coordinate s measured relative to the vertex of the cone, the solution set for membrane stress resultants and deformations in the cone becomes [28]

$$N_s = \frac{1}{s}\int (p_r \cot \alpha - p_s) s \; ds + k \tag{3a}$$

$$N_\theta = s\,(\cot \alpha) p_r \tag{3b}$$

$$\delta = \frac{1}{Et}(s \cos \alpha)(N_\theta - \nu N_s) \tag{3c}$$

$$V = \cot \alpha \left[\frac{1}{Et}(1+\nu)(N_s - N_\theta) - s\frac{d}{ds}\left\{\frac{1}{Et}(N_\theta - \nu N_s)\right\}\right] \tag{3d}$$

For the spherical shell under uniform external pressure, $r_1 = r_2 = a$, while $p_r = -p$ and $p_\phi = 0$. The constant of integration in equation (2a) is evaluated from the finiteness condition for N_ϕ at $\phi = 0$. The results for membrane stress resultants at generalised locations defined by the co-ordinate ϕ, as well as for membrane deformations evaluated at the edge of the spherical shell (defined by $\phi = \phi_e$) are as follows:

$$N_\phi^m = N_\theta^m = -\frac{pa}{2} \tag{4a}$$

$$\delta_1^m = -\frac{pa^2}{2Et}(1-\nu)\sin\phi_e = -\frac{pa^2}{2Et}(1-\nu)\sin\alpha \tag{4b}$$

$$V_1^m = 0 \tag{4c}$$

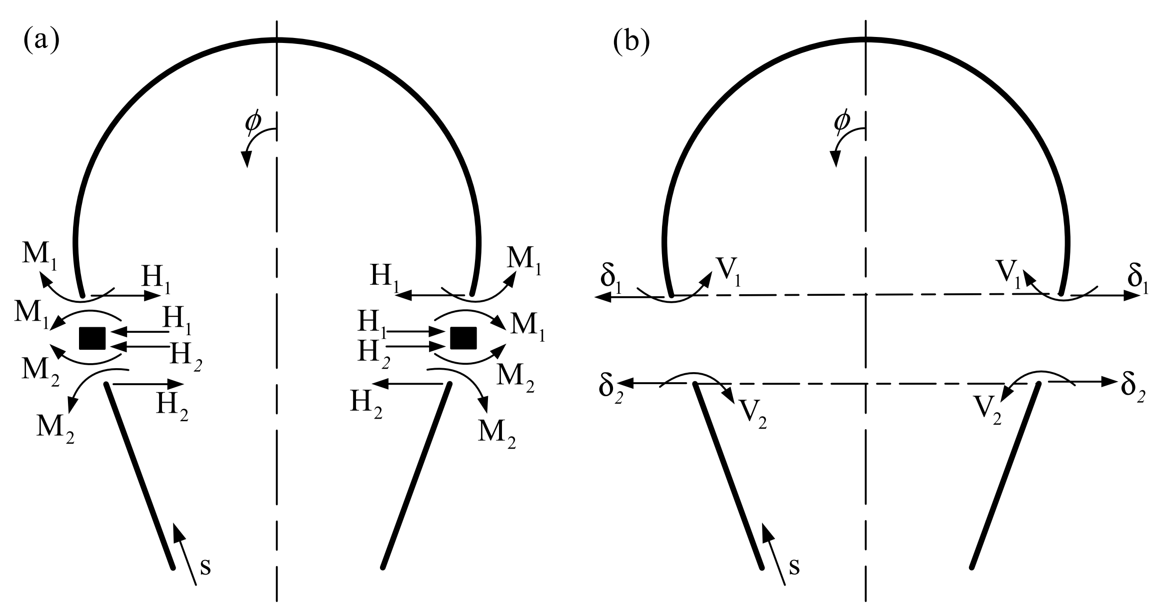

Fig. 2. Shell-edge actions and deformations: (a) actions on shell edges and reactions on an inter-shell element; (b) deformations at the shell edges.

noting that $\sin\phi_e = \sin\alpha$ since $\alpha = \pi - \phi_e$. The edge of the spherical shell is taken as "edge 1", hence the subscript 1; the superscript m denotes that these quantities relate to the membrane solution.

For the conical shell under uniform external pressure, $p_r = -p$ and $p_s = 0$. The constant of integration in equation (3a) is evaluated either by imposing the finiteness condition for N_s at $s = 0$ (vertex of the cone), or imposing the equality of N_s (in the conical shell) and N_ϕ (in the spherical shell) at the junction of the two shells. The results for membrane stress resultants at generalised locations defined by the coordinate s, as well as for membrane deformations evaluated at the edge of the conical shell (defined by $s = l$), are as follows:

$$N_s^m = -\frac{ps}{2}\cot\alpha \tag{5a}$$

$$N_\theta^m = -\ ps\ \cot\alpha \tag{5b}$$

$$\delta_2^m = -\frac{pl^2}{2Et}\left(\frac{\cos^2\alpha}{\sin\alpha}\right)(2-\nu) = -\frac{pa^2}{2Et}(\sin\alpha)(2-\nu) \tag{5c}$$

$$V_2^m = \frac{3}{2}\frac{pl}{Et}\cot^2\alpha = \frac{3}{2}\frac{pa}{Et}\cot\alpha \tag{5d}$$

noting that $l = a/\cot\alpha$; the edge of the conical shell is taken as "edge 2", hence the subscript 2.

3. Bending at the junction of the two shells

The Reissner-Meissner differential equations for the axisymmetric bending of general shells of revolution [3,4], when the shell thickness t is constant, simplify to

$$\frac{d^2V}{d\phi^2} + (\cot\phi)\frac{dV}{d\phi} - \left(\nu + \cot^2\phi\right)V = -\frac{a^2}{D}Q_\phi \tag{6a}$$

$$\frac{d^2Q_\phi}{d\phi^2} + (\cot\phi)\frac{dQ_\phi}{d\phi} + \left(\nu - \cot^2\phi\right)Q_\phi = EtV \tag{6b}$$

for the spherical shell, and

$$\frac{d^2V}{ds^2} + \frac{1}{s}\frac{dV}{ds} - \frac{1}{s^2}V = -\frac{Q_s}{D} \tag{7a}$$

$$\frac{d^2Q_s}{ds^2} + \frac{3}{s}\frac{dQ_s}{ds} = \frac{1}{s^2}\left(\tan^2\alpha\right)EtV \tag{7b}$$

for the conical shell, where the variable Q_ϕ (in the case of the spherical shell) or Q_s (in the case of the conical shell) denotes the transverse shear force per unit length as seen in the meridional section of the shell, and the parameter D denotes the flexural rigidity of the shell, defined as

$$D = \frac{Et^3}{12(1-\nu^2)} \tag{8}$$

For shells of revolution of positive Gaussian curvature and zero Gaussian curvature, if the shell is sufficiently thin (i.e. $a/t \geq 50$ for spherical shells and $r_2/t \geq 50$ for conical shells), and the shell sides are sufficiently steep in the region of the shell edge (i.e. $90^\circ < \phi_e \leq 135^\circ$ for the spherical shell and $45^\circ \leq \alpha < 90^\circ$ for the conical shell), we may discard terms in the zeroth and first derivatives, and retain only terms in the second derivatives. These simplifications, as applied to the spherical shell, are referred-to in shell literature as the Geckeler approximation. As shown in a previous study [29], the accuracy of the Geckeler approximation is primarily a function of the a/t ratio of the shell and the meridional angle ϕ_e of the shell at the edge in question. These conditions are amply fulfilled in the present problem, where the steel shell is generally quite thin ($a/t \geq 150$), and the opening angle of the spherical shell is generally chosen in the range $100^\circ \leq \phi_e \leq 120^\circ$ (so that $60^\circ \leq \alpha \leq 80^\circ$).

For the spherical shell, the Geckler approximation allows the simplified equations to be combined into a single fourth-order differential equation in the variable Q_ϕ [28]:

$$\frac{d^4Q_\phi}{d\phi^4} + 4\lambda^4\ Q_\phi = 0 \tag{9}$$

where the parameter λ is defined by the equation

$$\lambda^4 = 3\left(1-\nu^2\right)\left(\frac{a}{t}\right)^2 \tag{10}$$

The general solution of equation (9) has, of course, four constants of integration. These allow four boundary conditions to be specified at the two edges of a shell frustum [30,31], which may be decoupled with insignificant loss of accuracy if the two edges are sufficiently distanced from each other [30], or reduced to two equivalent boundary conditions if the frustum happens to have a mirror plane of symmetry [31]. In the present problem, both the spherical shell and the conical shell only have one edge (i.e. the location at which the two shells meet), so only two constants of integration are required for each shell. The solution of equation (9) may therefore be taken in the form [28]

$$Q_\phi = Ce^{-\lambda\psi}\sin(\lambda\psi + \beta) \tag{11}$$

where C and β are constants to be determined from the static boundary conditions at the edge, and ψ is the angular coordinate measured relative to the shell edge (i.e. $\psi = \phi_e - \phi$). Consider the application of an axisymmetric bending moment M_1 (per unit length) and horizontal shear force H_1 (per unit length) at the edge of the spherical shell, as shown in Fig. 2(a). The ensuing stress resultants N_ϕ^b and N_θ^b (the superscript b denoting that these variables are associated with the bending or edge effect) and bending moments M_ϕ and M_θ in the spherical shell are given by the expressions [28]

$$N_\phi^b = -\{\cot(\phi_e - \psi)\}\, e^{-\lambda\psi}\left\{\frac{2\lambda}{a}(\sin\lambda\psi)M_1 - (\sin\phi_e)(\sin\lambda\psi - \cos\lambda\psi)H_1\right\} \tag{12a}$$

$$N_\theta^b = -\ e^{-\lambda\psi}\left\{\frac{2\lambda^2}{a}(\sin\lambda\psi - \cos\lambda\psi)M_1 + 2\lambda(\sin\phi_e)(\cos\lambda\psi)H_1\right\} \tag{12b}$$

$$M_\phi = e^{-\lambda\psi}\left\{(\sin\lambda\psi + \cos\lambda\psi)M_1 - \frac{a}{\lambda}(\sin\phi_e)(\sin\lambda\psi)H_1\right\} \tag{12c}$$

$$M_\theta = \nu\ M_\phi \tag{12d}$$

while the deformations V_1^b and δ_1^b at the edge of the spherical shell, due to the actions M_1 and H_1, may be written as follows [28]:

$$\begin{bmatrix} V_1^b \\ \delta_1^b \end{bmatrix} = \begin{bmatrix} -\dfrac{4\lambda^3}{Eat} & \dfrac{2\lambda^2}{Et}(\sin\phi_e) \\ \dfrac{2\lambda^2}{Et}(\sin\phi_e) & -\dfrac{2\lambda a}{Et}(\sin^2\phi_e) \end{bmatrix}\begin{bmatrix} M_1 \\ H_1 \end{bmatrix} = \begin{bmatrix} I_{11} & I_{12} \\ I_{21} & I_{22} \end{bmatrix}\begin{bmatrix} M_1 \\ H_1 \end{bmatrix}. \tag{12e}$$

The positive sign convention for the deformations at the edges of the spherical shell and the conical shell is depicted in Fig. 2(b).

For the conical shell, Geckeler-type simplifications of equations (7) lead to the fourth-order differential equation [28]

$$\frac{d^4Q_s}{ds^4} + 4\eta^4 Q_s = 0 \tag{13}$$

where the parameter η is defined by the equation

$$\eta^4 = \frac{3(1-\nu^2)}{(l^2\cot^2\alpha)t^2} \tag{14}$$

In the cases where the conical shell has a single edge rather than two edges (i.e. a complete cone as opposed to a frustum), the solution of equation (13) may be taken in the form

$$Q_s = Ce^{-\eta x}\sin(\eta x+\xi) \tag{15}$$

where C and ξ are constants to be determined from the static boundary conditions at the edge of the cone, and x is the distance coordinate measured relative to the shell edge (i.e. $x = l - s$). For the application of an axisymmetric bending moment M_2 and horizontal shear force H_2 at the edge of the conical shell, as shown in Fig. 2(a), the ensuing stress resultants N_s^b and N_θ^b and bending moments M_s and M_θ in the conical shell are given by the expressions [28]

$$N_s^b = -(\cot\alpha)\, e^{-\eta x}\, \{2\eta\, (\sin\eta x)M_2 - (\sin\alpha)(\sin\eta x - \cos\eta x)H_2\} \tag{16a}$$

$$N_\theta^b = -(l\cot\alpha)e^{-\eta x}\{2\eta^2(\sin\eta x - \cos\eta x)M_2 + 2\eta(\sin\alpha)(\cos\eta x)H_2\} \tag{16b}$$

$$M_s = e^{-\eta x}\left\{(\sin\eta x+\cos\eta x)M_2 - \frac{1}{\eta}(\sin\alpha)(\sin\eta x)H_2\right\} \tag{16c}$$

$$M_\theta = \nu\, M_s \tag{16d}$$

while the deformations V_2^b and δ_2^b at the edge of the conical shell, due to the actions M_2 and H_2, may be written as [28]

$$\begin{bmatrix} V_2^b \\ \delta_2^b \end{bmatrix} = (l^2\cot^2\alpha)\begin{bmatrix} -\dfrac{4\eta^3}{Et} & \dfrac{2\eta^2}{Et}(\sin\alpha) \\ \dfrac{2\eta^2}{Et}(\sin\alpha) & -\dfrac{2\eta}{Et}(\sin^2\alpha) \end{bmatrix} \begin{bmatrix} M_2 \\ H_2 \end{bmatrix} = \begin{bmatrix} J_{11} & J_{12} \\ J_{21} & J_{22} \end{bmatrix}\begin{bmatrix} M_2 \\ H_2 \end{bmatrix}. \tag{16e}$$

It should be noted that for the present structural configuration where the spherical shell meets the conical shell at a tangent as illustrated in Fig. 1, the term $l\cot\alpha$ in relations (14), (16b) and (16e) may be replaced by a (the radius of the spherical shell), since $\tan\alpha = l/a$.

4. Solution for shell-edge redundants

Moment and horizontal-force equilibrium of an element between the two shells (refer to Fig. 2(a)) requires that

$$M_1 - M_2 = 0 \tag{17a}$$

$$H_1 + H_2 + (N_1^m - N_2^m)\cos\alpha = 0 \tag{17b}$$

While the bending actions at the edges of the two shells, i.e. $\{M_1, H_1\}$ for the spherical shell and $\{M_2, H_2\}$ for the conical shell, are shown in Fig. 2(a), the membrane meridional forces at the edges of the two shells, i.e. N_1^m for the spherical shell and N_2^m for the conical shell, are not shown to avoid congesting the diagram. Since membrane stress resultants are considered positive when tensile, the (action-and-reaction) biactions of N_1^m and N_2^m point towards each other, pulling *away* from the respective shell edge and inter-shell element. Vertical force equilibrium of the inter-shell element requires that N_1^m and N_2^m be equal to each other, a condition that is already fulfilled. Equations (17) therefore yield the relationships

$$M_2 = M_1 \tag{18a}$$

$$H_2 = -H_1 \tag{18b}$$

Continuity of rotations and lateral displacement across the junction of the two shells (refer to Fig. 2(b)) requires that

$$V_1^T = -V_2^T \tag{19a}$$

$$\delta_1^T = \delta_2^T \tag{19b}$$

where superscript T (for total) denotes the sum of membrane effects and bending edge effects:

$$V_1^T = V_1^b + V_1^m; \quad V_2^T = V_2^b + V_2^m \tag{19c}$$

$$\delta_1^T = \delta_1^b + \delta_1^m; \quad \delta_2^T = \delta_2^b + \delta_2^m \tag{19d}$$

We first substitute relations (19c) and (19d) into equations (19a) and (19b). In the ensuing expressions, we substitute the expressions for $\{V_1^b, \delta_1^b\}$ and $\{V_2^b, \delta_2^b\}$ as given by equations (12e) and (16e). This yields two equations each featuring all four bending actions M_1, H_1, M_2 and H_2. We make use of relations (18) to eliminate M_2 and H_2 from these equations, which finally become

$$\begin{bmatrix} (I_{11}+J_{11}) & (I_{12}-J_{12}) \\ (I_{21}-J_{21}) & (I_{22}+J_{22}) \end{bmatrix}\begin{bmatrix} M_1 \\ H_1 \end{bmatrix} = \begin{bmatrix} -(V_1^m+V_2^m) \\ (\delta_2^m - \delta_1^m) \end{bmatrix} \tag{20}$$

i.e.

$$\begin{bmatrix} A_{11} & A_{12} \\ A_{21} & A_{22} \end{bmatrix}\begin{bmatrix} M_1 \\ H_1 \end{bmatrix} = \begin{bmatrix} B_1 \\ B_2 \end{bmatrix} \tag{21}$$

where

$$A_{11} = (I_{11}+J_{11})\ ;\ A_{12} = (I_{12}-J_{12})\ ;A_{21} = (I_{21}-J_{21})\ ;A_{22} = (I_{22}+J_{22}) \tag{22a}$$

$$B_1 = -(V_1^m + V_2^m)\ ;\ B_2 = (\delta_2^m - \delta_1^m) \tag{22b}$$

The membrane edge deformations occurring in the expressions for B_1 and B_2 were given earlier as equations (4b), (4c), (5c) and (5d). Solving equation (21) for M_1 and H_1, we obtain

$$M_1 = \frac{B_1A_{22} - B_2A_{12}}{A_{11}A_{22} - A_{12}^2} \tag{23a}$$

$$H_1 = \frac{B_2A_{11} - B_1A_{12}}{A_{11}A_{22} - A_{12}^2} \tag{23b}$$

where use has been made of the relationship $A_{21} = A_{12}$. With the spherical-shell redundants M_1 and H_1 now known, the conical-shell redundants M_2 and H_2 immediately follow from relations (18).

5. Final shell stresses

When the solutions for the shell redundants $\{M_1, H_1, M_2, H_2\}$ are substituted into equations (12) for the spherical shell and (16) for the conical shell, we get values of stress resultants and bending moments in the shell due to edge effects. When the stresses associated with the edge effects are superimposed with the stresses associated with the membrane solution, we get the final shell stresses in the meridional and hoop directions as follows [28]:

$$\text{Spherical shell: } \sigma_\phi^T = \frac{N_\phi^m}{t} + \frac{N_\phi^b}{t} \pm \frac{6M_\phi}{t^2};\ \sigma_\theta^T = \frac{N_\theta^m}{t} + \frac{N_\theta^b}{t} \pm \frac{6M_\theta}{t^2} \tag{24}$$

$$\text{Conical shell: } \sigma_s^T = \frac{N_s^m}{t} + \frac{N_s^b}{t} \pm \frac{6M_s}{t^2};\quad \sigma_\theta^T = \frac{N_\theta^m}{t} + \frac{N_\theta^b}{t} \pm \frac{6M_\theta}{t^2} \tag{25}$$

Regarding the ± symbols appearing in these final expressions, the upper sign refers to the inner surface of the shell, while the lower sign refers to the outer surface.

6. Numerical examples

Let us consider a spherical-conical shell structure with the following geometrical parameters:

Spherical shell: $a = 5.0\text{m}$; $\phi_e = 105^\circ$; $t = 20\text{mm}$; $a/t = 250$.

Conical shell: $\alpha = 75^\circ$; $l = a\tan\alpha = 18.660\text{m}$; $t = 20\text{mm}$; $r_2/t = 250$ (at base of cone).

Let us assume the material parameters for both shells are those for steel, namely:

$$E = 205 \times 10^9 \text{N/m}^2 \ ; \ \nu = 0.3$$

Let us consider the situation of submergence of the structure in 100m of water. We will take the external hydrostatic pressure to be constant and given by

$$p = \gamma h = \left(10\text{kN/m}^3\right)(100\text{m}) = 10^6 \text{N/m}^2$$

Using equations (10) and (14), the slenderness parameters of the two shells are obtained as

$$\lambda = 20.324069 \ ; \ \eta = 4.064814\text{m}^{-1}$$

The membrane parameters B_1 and B_2 are calculated from equations (22b):

$$B_1 = -\ 0.490151 \times 10^{-3} \ ; \ B_2 = -\ 2.944896 \times 10^{-3}\text{m}$$

The influence coefficients for the two shells, I_{ij} and J_{ij} ($i = 1, 2$; $j = 1, 2$), are evaluated from equations (12e) and (16e). The results are:

$$I_{11} = -1.638091 \times 10^{-6}\text{N}^{-1} \ ; \ I_{12} = I_{21} = 0.194631 \times 10^{-6}\text{mN}^{-1} \ ; \ I_{22} = -\ 0.0462503 \times 10^{-6}\text{m}^2\text{N}^{-1}$$

$$J_{11} = -1.638092 \times 10^{-6}\text{N}^{-1} \ ; \ J_{12} = J_{21} = 0.194631 \times 10^{-6}\text{mN}^{-1} \ ; \ J_{22} = -\ 0.0462503 \times 10^{-6}\text{m}^2\text{N}^{-1}$$

The parameters A_{ij} ($i = 1, 2$; $j = 1, 2$) follow from equations (22a) as

$$A_{11} = -\ 3.276182 \times 10^{-6}\text{N}^{-1} \ ; \ A_{12} = A_{21} = 0 \ ; \ A_{22} = -\ 0.0925006 \times 10^{-6}\text{m}^2\text{N}^{-1}.$$

With the B_i ($i = 1, 2$) and A_{ij} now known, the values of the redundants (edge actions) follow from equations (23) and (18):

$$M_1 = M_2 = 149.61 \ \text{Nm/m} \ ; \ H_1 = -H_2 = 31,836.5 \ \text{N/m}$$

Use of these values into equations (12) and (16), and combining the associated stresses with their membrane counterparts in accordance with equations (24) and (25), then yields total stresses.

Analytical results for meridional and hoop stress variations, calculated on the basis of equations (24) and (25), are shown in Fig. 3 for the regions of the two shells that are adjacent to the junction. The horizontal ordinate is the cumulative distance measured from the crown of the vessel along the spherical-shell meridian, through the junction and along the conical-shell meridian towards the vertex of the cone at the bottom. Thus the cumulative distance coordinate of the junction is 9.163 m (the location of the junction is marked by the faint vertical line in the plots), while the cumulative distance coordinate of the vertex of the cone (not shown in the figure) is 27.823 m. The grey plot line relates to the membrane stress (constant across the shell thickness), the orange plot line relates to the total stress on the inner surface of the shell, and the blue plot line relates to the total stress on the outer surface of the shell.

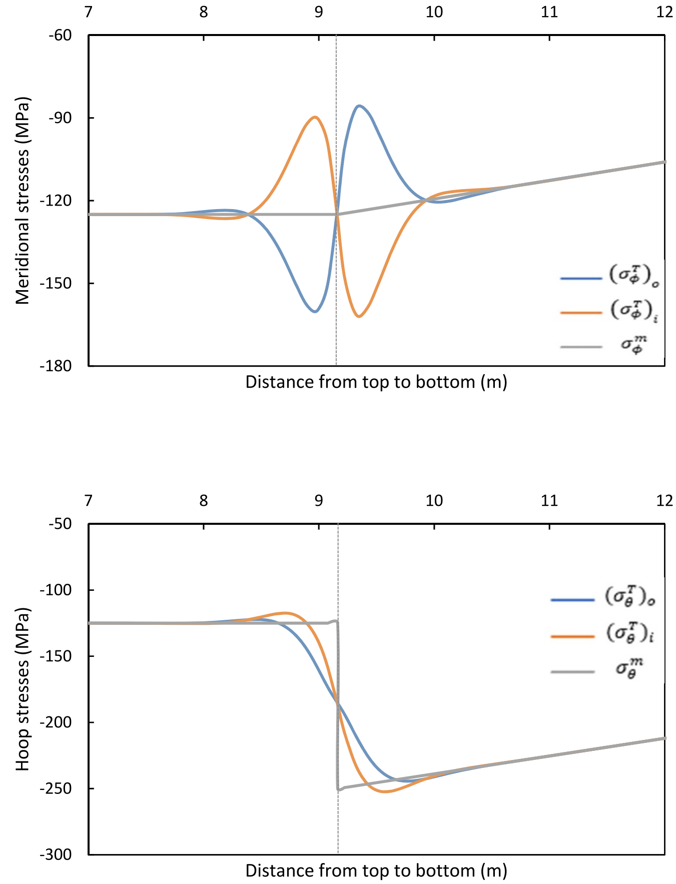

Fig. 3. Analytical plots of stress variations in the edge zone of vessel 1.

The same problem was also modelled using the finite-element programme ABAQUS [32]. For this analysis, a 3-node quadratic axisymmetric shell element (SAX2) was adopted. This has three degrees of freedom per node (two translations and one rotation). For the mesh, an element length of 0.2 m sufficed throughout the vessel, but this was reduced to 0.05 m in the edge zones of the two shells. As self-weight is neglected, and uniform external pressure is assumed, the net downward force on the structure should be zero, and no external supports should be required. In practice, the external hydrostatic pressure, while only varying by a relatively small amount across the depth of the vessel, has a net upward resultant tending to push the vessel towards the surface, so the vessel has to be fitted with ballast tanks at the bottom of the cone to keep it at a constant depth, or it has to be tied to the sea bed by a cable attached to the vertex of the cone. The latter condition may be simulated (in the FEM model) by restraining the vertical translation at the lowest point of the vessel. The horizontal translation was also restrained at the two poles of the vessel (i.e. at the points where the axis of revolution of the shell assembly intersects the shell wall).

Fig. 4 shows plots of FEM stress variations juxtaposed against their analytical counterparts, for ease of comparison. The FEM plots do not, of course, feature the grey line for membrane stresses, since it is the final stresses that matter in an FEM analysis. Comparing the analytical versus the FEM plots, it is evident that the results are practically identical throughout the domain of the vessel, confirming the high degree of accuracy of the theory that has been presented, despite its approximate nature.

A second numerical example was considered, by making the spherical shell a little deeper at $\phi_e = 120^\circ$, while still keeping the radius at $a = 5.0$ m and the shell thickness at $t = 20$ mm. The tangential cone therefore has sides of reduced slope $\alpha = 60^\circ$ and shorter length $l = 8.660$ m. The purpose of this variation was to establish to what extent the behaviour of the vessel was influenced by the location of the junction

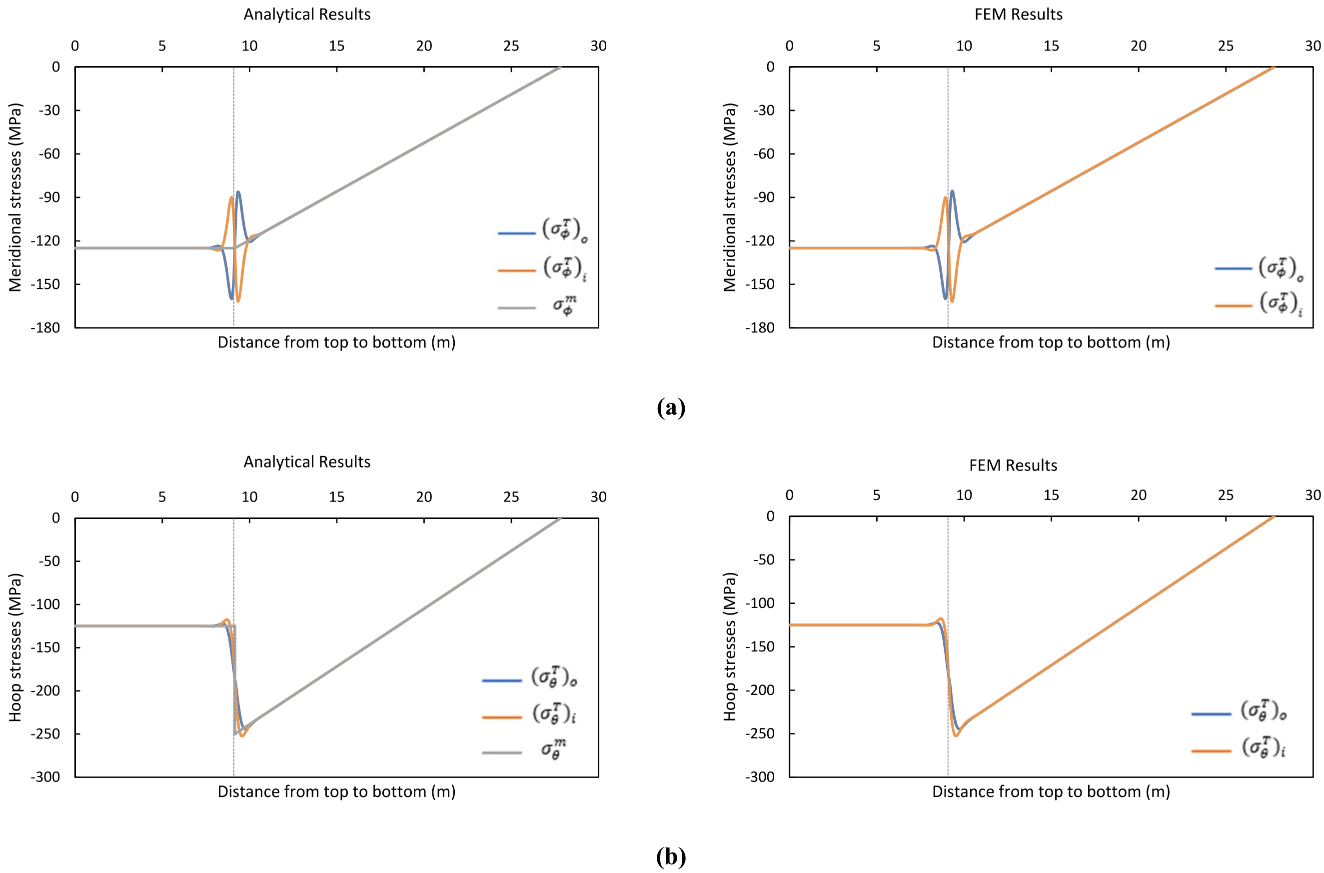

Fig. 4. Comparison of analytical versus FEM stress variations for vessel 1: (a) meridional-stress variation; (b) hoop-stress variation.

of the two shells as defined by the parameter ϕ_e. For the purposes of the discussion that follows, we will refer to the original example (with $\phi_e = 105^\circ$, $\alpha = 75^\circ$ and $l = 18.660$ m) as vessel 1, and the second example (with $\phi_e = 120^\circ$, $\alpha = 60^\circ$ and $l = 8.660$ m) as vessel 2.

For both examples, the membrane solution is seen to give uniform compressive stresses of 125 MPa throughput the spherical shell. In crossing the junction into the conical shell, membrane meridional stresses start off at a compressive value of 125 MPa and, of course, reduce linearly to zero as we move towards the vertex of the cone. On the other hand, there is a sudden jump in the membrane hoop-stress variation at the junction, from 125 MPa (compressive) on the spherical side to 250 MPa (compressive) on the conical side. From there, the membrane hoop-stress variation in the cone reduces linearly to zero as the vertex of the cone is approached. Of all locations, the edge of the cone therefore experiences the largest compression. These are trivial observations that are immediately evident from the membrane solution (equation (4) and (5)).

What is more significant is that the bending disturbance at the junction of the two shells induces additional stresses that result (i) in sharp localised peaks in the meridional-stress variation (these reach -160 MPa in the spherical shell and -161 MPa in the conical shell for vessel 1, and -158 MPa in the spherical shell and -162 MPa in the conical shell for vessel 2), and (ii) in a smoothening of the membrane hoop-stress jump between the two shells, which leaves the magnitude of the net hoop stresses in the vicinity of the junction essentially the same as the calculated membrane hoop stress at the edge of each shell. Furthermore, the lowering of the location of the spherical-conical junction from $\phi_e = 105^\circ$ to $\phi_e = 120^\circ$ has little effect on the magnitude of the edge effects; net stresses remain essentially the same. Also, the extent (or effective range) of the bending disturbance in the spherical shell and the conical shell remains essentially the same in moving from the configuration of vessel 1 to that of vessel 2. This is because the effective range of the bending disturbance is inversely proportional to the shell slenderness parameter λ in the case of the spherical shell and η in the case of the conical shell [28], and these shell parameters, being only functions of a, t and ν in the present problem, remain the same for the two examples (recalling that for the conical shell, $l \cot \alpha = a$).

The magnitude of the net hoop compressive stresses around the opening of the conical shell (essentially equal to the membrane value of 250 MPa) is the largest in compression in the entire assembly, which informs us that the edge region of the conical shell is the zone that is most likely to be the first to be affected by buckling, given that the two shells have the same thickness.

7. Buckling studies

A linear eigenvalue buckling analysis was performed for the two configurations of spherical-conical vessels. For the modelling, the S4R quadrilateral element of ABAQUS [32] was employed. This is a doubly curved thin-shell element with 6 degrees-of-freedom at each node, and thus capable of capturing non-axisymmetric behaviour (buckling typically breaks the axisymmetry of the shell, though some modes may still exhibit axisymmetry). As for the stress analysis, element sides of the order of 0.2 m were adopted throughout the vessel, these being suitably reduced to the order of 0.05 m in the edge zones of the two shells. Selected results for the obtained buckling modes and associated buckling pressures are shown in Fig. 5 (for vessel 1) and Fig. 6 (for vessel 2). For each of the selected modes, the diagram on the left is a side view of the deformed vessel, while that on the right is the view of the vessel looking upwards from below the vertex of the cone.

For vessel 1 (with $a = 5$m, $t = 20$mm, $\phi_e = 105^\circ$, $\alpha = 75^\circ$ and $l = 18.660$ m), the lowest buckling pressure is obtained as 0.147MPa,

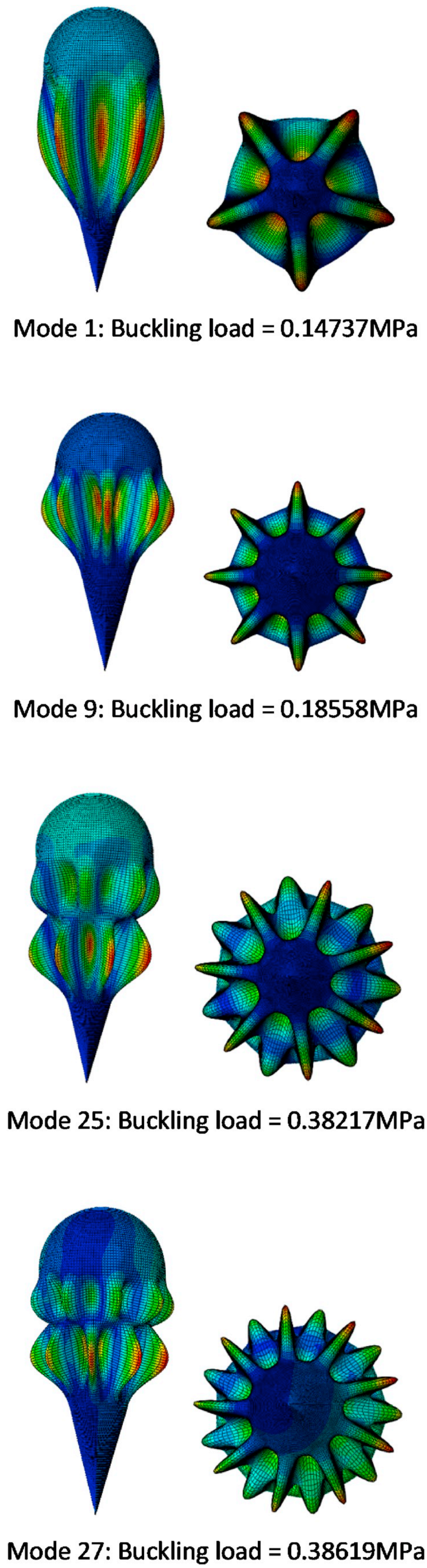

Fig. 5. Buckling modes of vessel 1.

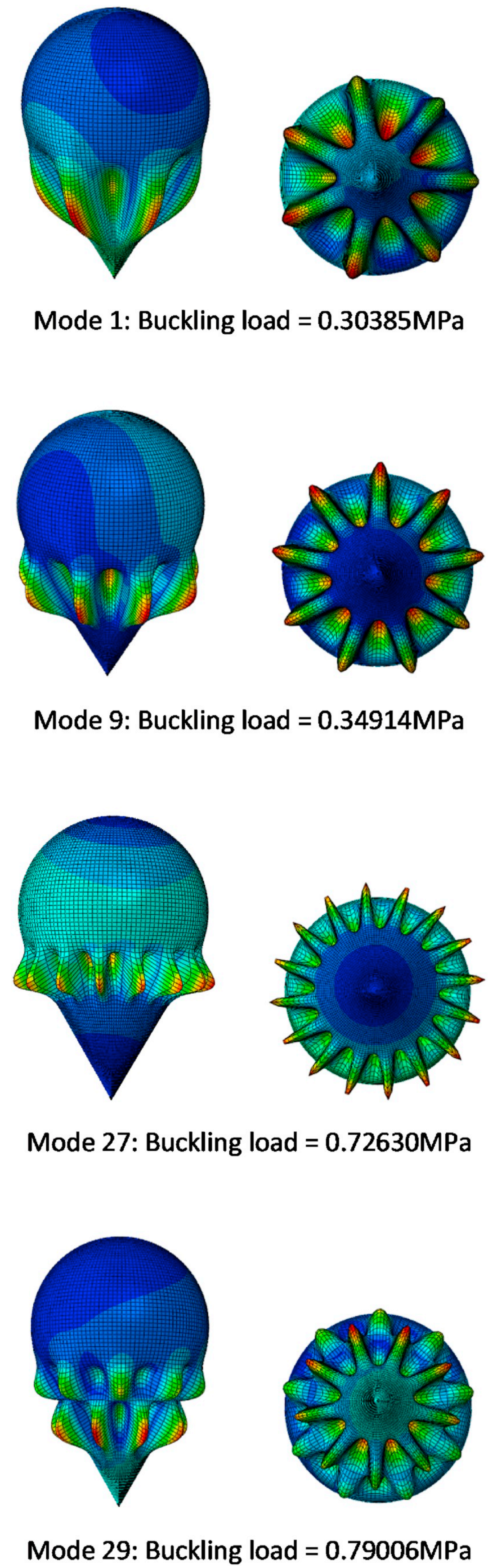

Fig. 6. Buckling modes of vessel 2.

which is a relatively low buckling resistance (the equivalent of only 14.7m head of water). This is characterised by 5 circumferential waves and one longitudinal wave in the upper region of the conical vessel, a result consistent with the predictions of the last section. Higher modes are also characterised by multiple circumferential waves and a single longitudinal wave generally affecting the upper regions of the conical shell, until mode 23 is reached, when two waves begin to emerge in the longitudinal direction. Eigenvalues (buckling pressures) occur in identical pairs (this is typical of structures with symmetry, in this case axisymmetry), with adjacent values being relatively close to each other. For instance, modes 29 and 30 each exhibit 14 circumferential waves and one relatively short wave adjacent to the edge of the conical shell, the associated buckling pressure being still a modest 0.391MPa (the equivalent of 39.1m of water).

For vessel 2 (with $a = 5$m, $t = 20$mm, $\phi_e = 120^\circ$, $\alpha = 60^\circ$ and $l = 8.660$ m), by extending the spherical shell a little further down (at the expense of the conical shell that becomes less steep and shorter), we find that the lowest buckling pressure increases by as much as 107% to 0.304MPa, and this is characterised by 7 circumferential waves and one longitudinal wave over the conical shell. Higher modes follow trends similar to those of vessel 1, with these generally having one or two more circumferential waves than their vessel-1 counterparts. For vessel 2, the number of longitudinal waves increases to 2 only when mode 29 is reached. Even for such a high mode number, the buckling pressure is only 0.790MPa (79m of water).

Replacing the conical shell of vessel 1 with a paraboloid of revolution that has the same slope as the conical shell at the junction with the spherical shell, and by reference to equation (1), we get $k = 0.38637$. The depth of the paraboloid of revolution follows as $h = 9.012$m. For the parabolic variant of vessel 2, we get $k = 0.20$ and $h = 3.75$m. We will refer to the parabolic variants of vessels 1 and 2 as vessels 3 and 4 respectively. Selected results for buckling modes and associated buckling pressures for vessels 3 and 4 are shown in Fig. 7.

For the same mode numbers, the parabolic variant of the spherical-conical vessel exhibits a substantially higher buckling capacity than its conical counterpart (by virtue of double curvature), and the number of circumferential waves tend to be higher. Thus, the lowest buckling pressure of vessel 3 becomes 0.379MPa (158% higher than that of vessel 1), while that of vessel 4 becomes 1.109MPa (265% higher than that of vessel 2). The benefits of double curvature are clearly evident, albeit at the expense of loss of height of the lower shell. However, the parabolic shell is still weaker than the spherical shell above it; all the buckling is confined to the lower shell, with the spherical shell remaining stable well beyond mode 30.

It is interesting to compare the surface areas and volumes of vessels 1 to 4. These are shown in Table 1. The stress and buckling analyses ignore the effects of self-weight (as these are insignificant in comparison with the effects of hydrostatic pressure), but nonetheless the masses of the vessels (which are proportional to surface area) have been computed assuming a density of 7800kg/m^3 for the steel, and are included in the table. From an operational and functional point of view, vessel 3 (the parabolic variant of vessel 1) has the advantage of having the least surface-area-to-volume ratio of 0.574, while also offering a relatively large internal volume (691.37m^3) and a sufficiently extended depth (15.306m) for good underwater observations. Although vessel 4 has the advantages of least mass and highest buckling resistance, it has the disadvantages of having the least internal volume (552.23m^3) and the least vertical extent (11.25m).

8. Concluding remarks

In this paper, externally pressurised spherical-conical vessels have been investigated for possible deployment in shallow sea water. A formulation for the calculation of discontinuity stresses at the junction of the two shells has been presented, and numerical examples

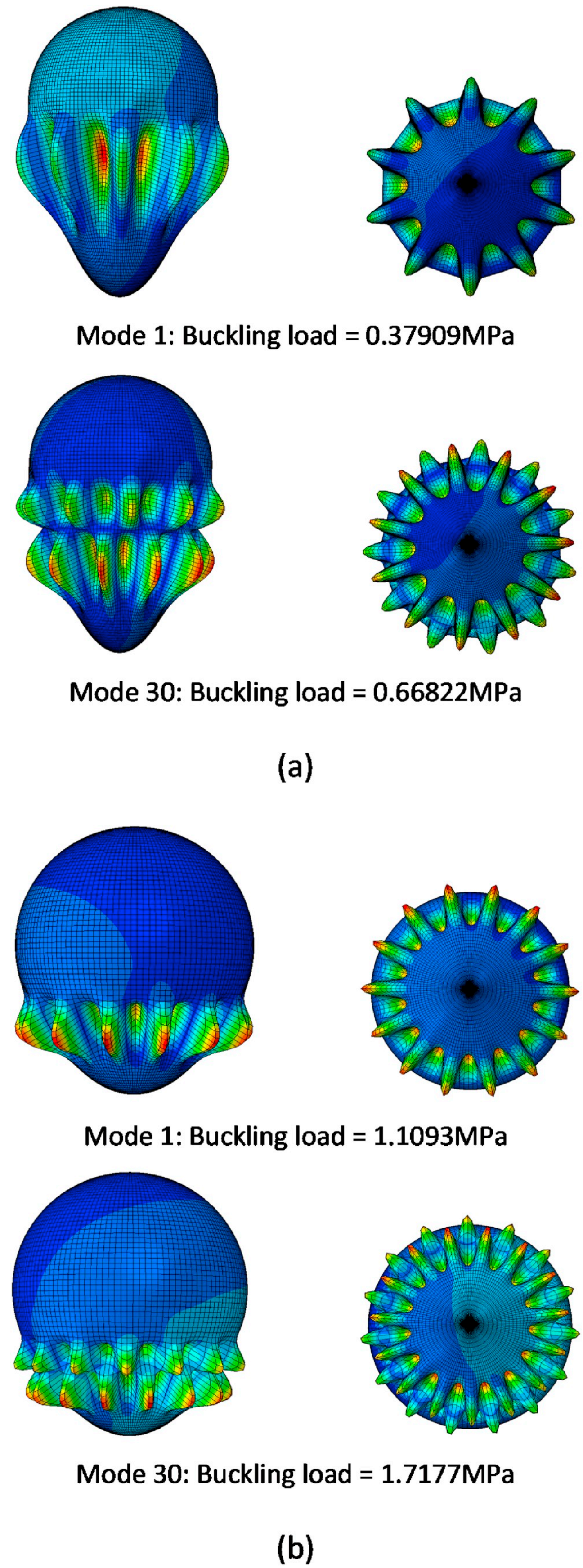

Fig. 7. Buckling modes of the parabolic variants: (a) vessel 3; (b) vessel 4.

Table 1
Surface areas, internal volumes and masses of the four vessels.

	vessel 1 (spherical-conical)	vessel 2 (spherical-conical)	vessel 3 (spherical-parabolic)	vessel 4 (spherical-parabolic)
surface S (m^2)	480.86	353.43	396.53	327.25
volume V (m^3)	801.44	589.05	691.37	552.23
S/V ratio (m^{-1})	0.600	0.600	0.574	0.593
mass M (kg)	75 014	55 135	61 859	51 051

considered. The state of stress throughout the vessel is compressive. While discontinuity effects result in sharp peaks of net meridional stresses that are 30% higher than the general level of membrane meridional stresses around the junction, they only have a smoothening effect on the net hoop-stress variation across the junction. As the magnitude of the membrane hoop stress in the conical shell is twice that in the spherical shell, the membrane value of the hoop stress at the opening of the conical shell provides a close upper-bound of the maximum compressive stresses in the entire vessel.

The linear elastic buckling analysis of the vessel has shown that buckling is confined to the conical shell, a finding that is consistent with the predictions of the stress analysis. The fact that buckling deformations generally initiate in the regions of the conical shell that are adjacent to the opening of the conical shell suggests that discontinuity effects at the junction of the two shells have an influence on the buckling behaviour of the vessel, but this could simply be due to the fact that the cone has the least stiffness (largest value of r_2) in this region. The relationship between buckling modes and discontinuity effects needs to be investigated in more detail. Further work is currently in progress in this regard.

What is clear is that buckling modes are generally characterised by several circumferential waves and a single longitudinal wave, a behaviour similar to that observed for many other shells of revolution [19–22]. The number of longitudinal waves only increases to 2 when the mode number becomes relatively high. Eigenvalues (buckling pressures) have been found to occur in identical pairs, and the calculated values tend to be very close to each other (very little spread of values between mode 1 and mode 30), which is typical of structures with symmetry [33–36].

Extending the spherical shell to deeper levels (hence making the cone less steep and shorter in length) results in a significant enhancement of the buckling capacity of the vessel, which still buckles in the conical part. Further enhancement of the buckling capacity occurs when the conical shell is replaced with the inscribed paraboloid of revolution.

A number of new research questions arise from the above results. In particular, is there a correlation between the shell slenderness parameter λ (or η) and the number of circumferential waves associated with the first elastic buckling mode? Should the oscillating but rapidly decaying bending-disturbance elastic deformations δ^b and V^b be taken into account (as some kind of axisymmetric geometric imperfections) in modelling the buckling behaviour of the vessel?

It should be stressed that the above conclusions are based on a linear buckling analysis of the shell. As pointed out earlier, the buckling load calculated in this way is not necessarily the collapse load; in reality, the shell may either fail abruptly as soon as buckling has occurred, or it may continue to carry an increasing amount of load while sustaining more severe deformations until it eventually collapses. The investigation is currently being extended to take into account non-linearity effects, postbuckling and collapse behaviour. The results will be published in a follow-up paper. Also, the focus has been on the perfect shell, and geometric imperfections have not been taken into account. The sensitivity of the buckling behaviour of the vessel to the presence of geometric imperfections will form the subject of future work. In the underwater environment, the geometry of the imperfections can evolve with time due to creep, corrosion or abrasion effects, so long-term structural performance [37] will need to be taken into account as well.

Acknowledgements

The authors wish to thank Kenny Mudenda (University of Cape Town) and Grant Kucherera (formerly of the University of Cape Town) for their assistance with the checking of the numerical modelling. Chisanga Kaluba (postgraduate student at the University of Cape Town) helped to improve the quality of some of the drawings, for which the authors are most grateful.

Appendix A. Supplementary data

Supplementary data to this article can be found online at https://doi.org/10.1016/j.tws.2019.106472.

References

[1] A.S. Tooth, in: "Storage Vessels", Developments in Thin-Walled Structures, vol. 1, Elsevier Applied Science, London, 1982, pp. 1–52.
[2] A. Zingoni, Liquid-containment shells of revolution: a review of recent studies on strength, stability and dynamics, Thin-Walled Struct. 87 (2015) 102–114.
[3] W. Flugge, Stresses in Shells, Springer-Verlag, Berlin, 1973.
[4] A. Zingoni, Shell Structures in Civil and Mechanical Engineering: Theory and Closed-form Analytical Solutions, Thomas Telford Publishing, The Institution of Civil Engineers, London, 1997.
[5] A. Zingoni, Stresses and deformations in egg-shaped sludge digesters: membrane effects, Eng. Struct. 23 (11) (2001) 1365–1372.
[6] A. Zingoni, Stresses and deformations in egg-shaped sludge digesters: discontinuity effects, Eng. Struct. 23 (11) (2001) 1373–1382.
[7] A. Zingoni, Discontinuity effects at cone-cone axisymmetric shell junctions, Thin-Walled Struct. 40 (10) (2002) 877–891.
[8] A. Zingoni, B. Mokhothu, N. Enoma, A theoretical formulation for the stress analysis of multi-segmented spherical shells for high-volume liquid containment, Eng. Struct. 87 (2015) 21–31.
[9] A. Zingoni, N. Enoma, N. Govender, Equatorial bending of an elliptic toroidal shell, Thin-Walled Struct. 96 (2015) 286–294.
[10] W. Pietraszkiewicz, V. Konopinska, Junctions in shell structures: a review, Thin-Walled Struct. 95 (2015) 310–334.
[11] T. Von Karman, H.S. Tsien, The buckling of spherical shells by external pressure, J. Aeronaut. Sci. 7 (1939) 43–50.
[12] J. Singer, Buckling of circular conical shells under axisymmetrical external pressure, J. Mech. Eng. Sci. 3 (1961) 330–339.
[13] P. Seide, On the buckling of truncated conical shells under uniform hydrostatic pressure, in: Proceedings of the IUTAM Symposium on the Theory of Thin Elastic Shells, North-Holland Publishing Company, Amsterdam, 1960, pp. 363–388.
[14] L.H. Sobel, W. Flügge, Stability of toroidal shells under uniform external pressure, Am. Inst. Aeronaut. Astronaut. (AIAA) J. 5 (1967) 425–431.
[15] S.N. Krivoshapko, Research on general and axisymmetric ellipsoidal shells used as domes, pressure vessels and tanks, Appl. Mech. Rev. 60 (2007) 336–355.
[16] J.G. Teng, Buckling of thin shells: recent advances and trends, Appl. Mech. Rev. 49 (1996) 263–274.
[17] E.M. Sosa, L.A. Godoy, Challenges in the computation of lower-bound buckling loads for tanks under wind pressures, Thin-Walled Struct. 48 (2010) 935–945.
[18] C.A. Burgos, R.C. Jaca, J.L. Lassig, L.A. Godoy, Wind buckling of tanks with conical roof considering shielding by another tank, Thin-Walled Struct. 84 (2014) 226–240.
[19] L.A. Godoy, Buckling of vertical oil storage steel tanks: review of static buckling studies, Thin-Walled Struct. 103 (2016) 1–21.
[20] J. Blachut, P. Smith, Buckling of multi-segment underwater pressure hull, Ocean. Eng. 35 (2008) 247–260.
[21] Q. Du, W. Cui, B. Zhang, Buckling characteristics of a circular toroidal shell with stiffened ribs, Ocean. Eng. 108 (2015) 325–335.
[22] W. Jiammeepreecha, S. Chucheepsakul, Nonlinear static analysis of an underwater elastic semi-toroidal shell, Thin-Walled Struct. 116 (2017) 12–18.
[23] P. Jasion, K. Magnucki, Elastic buckling of clothoidal-spherical shells under external pressure: theoretical study, Thin-Walled Struct. 86 (2015) 18–23.
[24] P. Jasion, K. Magnucki, Theoretical investigation of the strength and stability of special pseudospherical shells under external pressure, Thin-Walled Struct. 93 (2015) 88–93.
[25] A. Zingoni, N. Enoma, Strength and stability of externally pressurised spherical-conical shell assemblies, in: Eighth International Conference on Thin-Walled Structures (ICTWS 2018), 2018. Lisbon, Portugal, July 24-27.
[26] A. Zingoni, On membrane solutions for elevated shell-of-revolution tanks of certain meridional profiles, Thin-Walled Struct. 22 (2) (1995) 121–142.
[27] A. Zingoni, Parametric stress distribution in shell-of-revolution sludge digesters of parabolic ogival form, Thin-Walled Struct. 40 (7/8) (2002) 691–702.

[28] A. Zingoni, Shell Structures in Civil and Mechanical Engineering: Theory and Analysis, ICE Publishing, The Institution of Civil Engineers, London, 2018.
[29] A. Zingoni, M.N. Pavlovic, Computation of bending disturbances in axisymmetrically loaded spherical shells: a study of the accuracy of Geckeler's approximation, Eng. Comput. 7 (2) (1990) 125–143.
[30] A. Zingoni, M.N. Pavlovic, On edge-disturbance interaction and decoupling errors in thin-walled nonshallow spherical-shell frusta, Thin-Walled Struct. 13 (1992) 375–386.
[31] A. Zingoni, Simplification of the derivation of influence coefficients for symmetric frusta of shells of revolution, Thin-Walled Struct. 47 (2009) 912–918.
[32] ABAQUS Standard, Hibbit, Karlsson and Sorenson Inc, Newark (California), 1998.
[33] A. Zingoni, A group-theoretic finite-difference formulation for plate eigenvalue problems, Comput. Struct. 112/113 (2012) 266–282.
[34] Y. Chen, J. Feng, Generalized eigenvalue analysis of symmetric prestressed structures using group theory, J. Comput. Civ. Eng. 26 (4) (2012) 488–497.
[35] A. Zingoni, Group-theoretic insights on the vibration of symmetric structures in engineering, Phil. Trans. R. Soc. A 372 (2014), 20120037.
[36] Y. Chen, J. Feng, Q. Sun, Lower-order symmetric mechanism modes and bifurcation behavior of deployable bar structures with cyclic symmetry, Int. J. Solids Struct. 139/140 (2018) 1–14.
[37] A. Zingoni, Structural health monitoring, damage detection and long-term performance, Eng. Struct. 27 (12) (2005) 1713–1714.